Diamond-to-graphite conversion in nanodiamond and electronic properties of nanodiamond-derived carbon system

© T. Enoki

Department of Chemistry, Tokyo Institute of Technology,
Tokyo 152-8551, Japan

E-mail: tenoki@chem.titech.ac.jp

Heat-treatment-induced conversion of nanodiamond to nanographite is investigated. Graphitization starts at the surface region around a heat-treatment temperature of 900°C, then it proceeds inward in the particle, and finally it is completed around 1600°C, where nanographite particles form a polyhedron with a hollow inside. The change in the electronic feature is subjected to the structural change induced by the heat treat treatment. In the intermediate stage of graphitization, where graphene sheets are small and defective, charge transfer takes place from graphitic π-band to non-bonding edge states. Electrophoretic deposition of nanodiamond particles provides technique of fabricating isolated single nanodiamond particles on a substrate. Successive heat-treatment at 1600°C converts a nanodiamond particle to a single nanographene sheet laying flat on a highly oriented pyrolytic graphite substrate. Weak interaction between the nanographene sheet and the substrate is expected to give a model system of nanographene, for which theory predicts the presence of nonbonding π-electron states of the edge origin and its related unconventional nanomagnetism.

This work is supported by the Grant-in-Aid for „Research for the Future“ Program, Nano-Carbons and 15 105 005 from JSPS.

1. Introduction

Nanosized carbon systems such as fullerenes, carbon nanotubes and nanographene are of current interests in supramolecular chemistry, mesoscopic physics and molecular device applications. Among them, nanodiamond, whose structure is governed by the sp^3 carbon bond network, has unique features different from the other nanosized carbon systems having π-electron networks. In addition, the surface of nanodiamond is subjected to a structural reconstruction or the effect of functional groups attached to the surface. In case of diamond whose surface carbon atoms are bonded to hydrogen atoms, the electron emission is expected to be associated with negative electron affinity [1]. In the meantime, theoretical works have recently predicted the emergence of unconventional magnetism around the graphene/diamond interface [2]. In this context, it is interesting to investigate the conversion of nanodiamond to nanographite, where the interface between graphite and diamond phases is expected to impart structural and electronic features different from both phases. The finiteness in size is also considered to affect the conversion mechanism and resulting structures.

Another issue, which is challenging in nanoscience, is the fabrication of a single nanographene sheet, which is ascribed to the nanosized extreme of condensed polycyclic aromatic molecule in organic chemistry language, by using nanodiamond as a starting material. In recent theoretical and experimental works [3–6], it has been revealed that nanographene has the non-bonding π-electron state of the edge origin, which gives rise to the appearance of unconventional nanomagnetism.

In the present paper, we have investigated the process of the conversion of nanodiamond to nanographite in the heat-treatment temperature (HTT) range up to 1600°C from structural and electronic aspects, by means of X-ray diffraction, high resolution transmission electron microscope (HRTEM), scanning electron microscope (SEM), Raman scattering, scanning tunneling microscope (STM), atomic force microscope (AFM), magnetic susceptibility, and ESR. Electrophoretic deposition of nanodiamond and subsequent heat treatment was found to produce an isolated single nanographene sheet.

2. Heat-treatment-induced conversion of nanodiamond to nanographite

Diamond is converted to graphite thermally by the heat treatment. In such heat-treatment-induced conversion, nanodiamond behaves differently from bulk diamond due to the smallness of the particles. We have investigated the conversion process induced by heat-treatment of nanodiamond particles having a mean size of 5 nm in an argon atmosphere [5,7]. Raman spectra, which are sensitive to a presence of graphite with the G- and D-peaks located in the 1590 and 1350 cm^{-1} regions, respectively, prove the presence of graphitic ingredient even in the HTT range of 900°C, although no evidence of graphite is indicated in HRTEM and X-ray diffraction experiments. This suggests that only the surface region of nanodiamond particles is graphitized around that temperature, where nanographene domains are too small to be stacked as it is in bulk graphite. Graphitization proceeds inward upon further elevation of HTT at the expense of nanodiamond phase, as proved the appearance of graphitic structures in HRTEM and X-ray diffraction. Fig. 1 shows the variation of the structural parameters as a function of HTT. The graphite fraction grows steeply above ca 900°C and becomes 100% around HTT = 1600°C. The growth of in-plane size (L_a) is followed

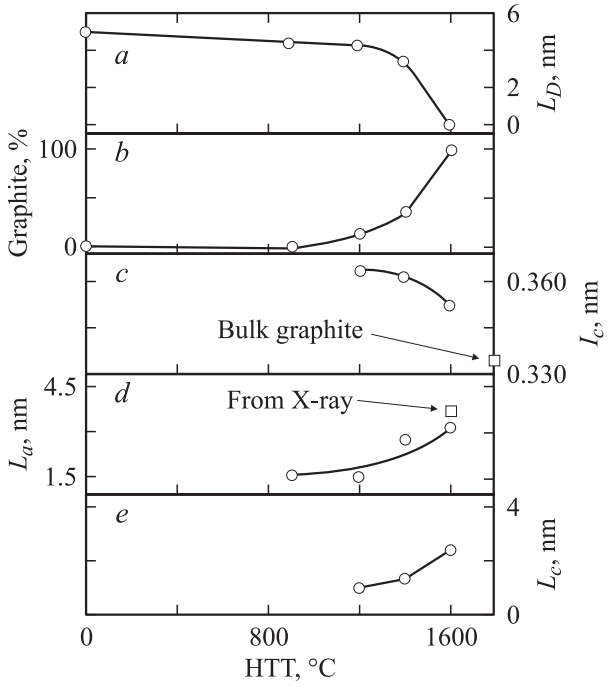

Figure 1. The variation of the structural parameters with HTT. (*a*) The diamond size (L_D), (*b*) the conversion ratio of diamond to graphite, (*c*) the observed graphite interlayer distance (I_c), (*d*) the graphite in-plane domain size (L_a), and (*e*) the graphite thickness along the *c*-axis (L_c).

by the development of *c*-axis stacking structure as evidenced in Fig. 1, *d* and *e*. At around HTT = 1600°C, where graphitization is completed, the size of nanographite becomes $L_a \times L_c = \text{ca}\,3 \times 2.5\,\text{nm}$, which gives a mean number of stacked graphene sheets of ca 7. HRTEM observations visualize the shape of nanographite particle obtained by the heat treatment at 1600°C. The particle forms a polyhedron with a mean size of 7–8 nm and a hollow inside, where each facet consists of a stacking of 3–7 graphene sheets, in good agreement with the *X*-ray diffractions. The interlayer distance I_c, which is a good indication of regularity of graphitic structure, is considerably larger than that of bulk graphite ($I_c = 0.3345\,\text{nm}$) in the beginning of graphitization around HTT = 1200°C, suggesting the presence of remnant corrugated features of the graphene sheets. The value of $I_c \sim 0.353\,\text{nm}$ at HTT = 1600°C is still larger than that of bulk graphite, though I_c decreases as the HTT is elevated. This is due to the turbostatic nature of the graphene sheets. Interestingly, the interlayer distance tends to be smaller as we go from the surface to the center of the polyhedron [8].

Next, we discuss the change in the electronic structure upon the heat treatment. The magnetic properties impart clues in characterizing the electronic properties. Fig. 2 presents the ESR linewidth ΔH, *g*-value, orbital susceptibility χ_{orb} and localized spin concentration n_s as a function of graphite fraction. The orbital susceptibility is negligibly small ($< 10^{-7}$ emu/g) for the samples with HTT < 900°C, suggesting the absence of an extended π-electron network. The increase in the graphite fraction upon the elevation of HTT rises the absolute value of χ_{orb} successively, and above HTT ≥ 1400°C, it becomes larger than that expected for the graphene sheet having the in-plane size obtained from the Raman spectra with the assumption that χ_{orb} of the samples can be obtained by extrapolating the values of condensed polycyclic aromatic hydrocarbons consisting of a small number of benzene rings. This means that the samples with HTT ≥ 1400°C have the extended π-electron system as bulk graphite has. However, the absolute value is still smaller than that of bulk graphite even at HTT = 1600°C. This is considered to be associated partly with the presence of remnant corrugation of graphene sheets. In addition to this, the anomalous electronic structure generated around the edges of nanographene, which is theoretically predicted as the non-bonding π-electron state of edge origin, can be also responsible for the modification of the orbital susceptibility. The Raman spectra give a hint in considering this context. Fig. 3 presents the positions of the *G*-peak, *D*-peak and the peak in the 1620 cm^{-1} region as a function of graphite fraction, which correspond the E_{2g2} mode, the disorder-induced line and a shoulder related to disorderness of graphite. The *G*-peak position is lower than that of bulk graphite in the samples with HTT < 900°C. This downshift is caused by bond angle disorder present in the sp^3-bonded

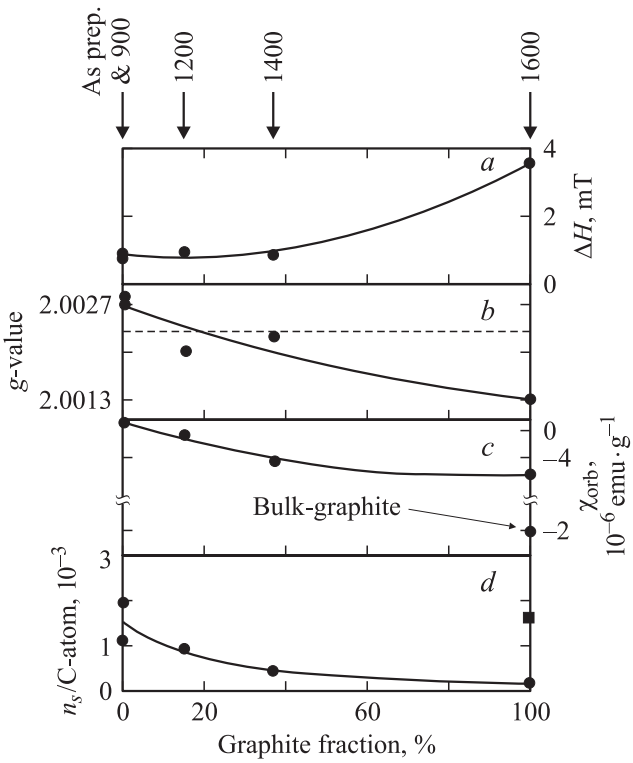

Figure 2. (*a*) The ESR linewidth ΔH, (*b*) *g*-value, (*c*) orbital susceptibility χ_{orb}, and (*d*) localized spin concentration per carbon atom n_s as a function of graphite fraction. The dashed line in (*b*) represents the *g*-value of free-electron spin. The full square at 100% in (*d*) is the estimate of the π-electron concentration. HTT is also given at the top of the figure.

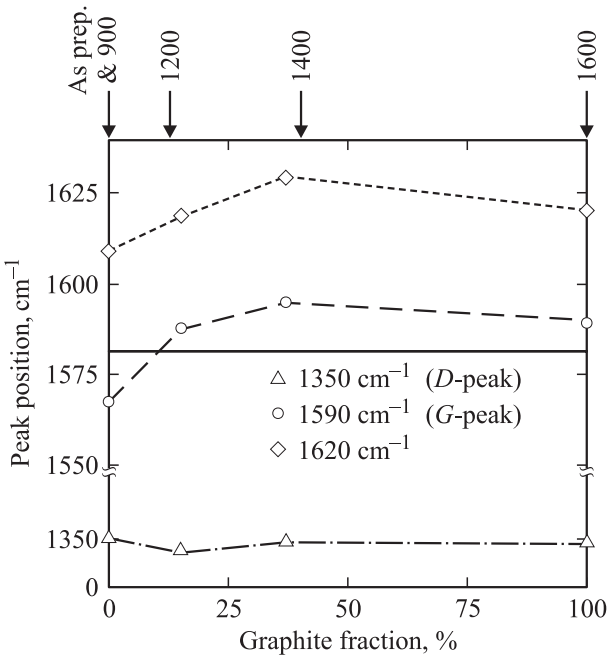

Figure 3. The peak position in Raman spectra as a function of the graphite fraction for 1350 cm^{-1} (D-peak), 1590 cm^{-1} (G-peak), and 1620 cm^{-1} (diamond) regions. The solid line is the peak position for the bulk graphite G-peak. HTT is also given at the top of the figure.

fraction that forces the graphene sheet to be nonplanar. The increase in the graphite fraction makes the peak position upshifted above the peak position of bulk graphite, resulting in stiffening the graphitic lattice. Such stiffening happens in general when charge transfer from acceptor to graphite makes the bonding π-band being partly vacant. According to previous works [3,4], non-bonding edge states are present around the peripheries of nanographene sheets. In the present samples, edge states are broadened by the structural disorder in the nanographite particles. Charge transfer from the π-band to the edge states generates holes, resulting the upshift of the G-peak, in addition to the reduction in the orbital susceptibility, demonstrating the importance of the edge states in the electronic structure of the nanographite. In this connection, it should be noted that the presence of holes is confirmed by thermoelectric power in nanographite [6].

Localized spins also reflect the electronic structure modified by the heat treatment. According to the spin concentration plotted as a function of graphite fraction shown in Fig. 2, *d*, the spin concentration decreases upon the increase in the graphite fraction. The nanodiamond particles as-prepared have many defects as they are prepared in nonequilibrium condition produced by explosion-induced transient high pressure. Therefore, a large number of defects are considered to be responsible for the localized spins for HTT $< 900^\circ$C. This is supported by the fact that the g-value is quite close to the g-value of microcrystalline diamond, where the spins are attributed to the paramagnetic centers created by the defects in the sp^3-network [9]. Further heat-treatment reduces the spin concentration with the ESR linewidth broadened and the g-values downshifted below the g-value of the free electron spins. In the sample of HTT $= 1600^\circ$C, where graphitization is completed, the ESR signal is split into sharp and broad signals with different g-values, which are assigned to the defect spins and π-electron spins, respectively. In the intermediate range with $1200 <$ HTT $< 1400^\circ$C, the graphene sheets are strongly corrugated with the presence of defects, in which the defects and π-electron spins are coupled to each other, giving rise to the linewidth broadening. Completion of graphitization wipes defects away from the extended π-electron region, resulting in the splitting of the ESR signal into the two peaks. Interestingly, the spin-lattice relaxation rate is accelerated above HTT $= 1400^\circ$C. In the sample with HTT $= 1600^\circ$C, the interaction between edge-state spins and conduction π-electro plays an important role in accelerating the spin-lattice relaxation process. In contract, the presence of defects hinders the interaction, the relaxation rate being slowed down.

3. Electrophoretic deposition of nanodiamond and formation of isolated single nanographene layer

Nanodiamond particles suspended in a solution can be electrophoretically deposited on a substrate in a controlled way for producing isolated single nanodiamond particles [10]. Successive heat treatment of isolated nanodiamond particles is expected to produce isolated nanographite particles on a substrate. Based on this procedure, we prepared isolated single nanographene sheet on a highly oriented pyrolytic graphite (HOPG) substrate. Diamond particles as-prepared are covered with functional groups containing oxygen such as carbonyl, carboxylic, lactone and epoxide. In aqueous and organic suspensions, the dissociation of surface carboxyl groups leads to the formation of negative charges. However, it is found that it is very difficult to isolate single particles due to the trend of clustering of particles.

The improved electrophoretic experiments are carried out with electrodes of HOPG, where nanodiamond particles are suspended in isopropyl alcohol solvent mixed with acetone, water and iodine as additives. Two HOPG electrodes with a size of $6 \times 5 \times 0.5$ mm are placed apart from each other by 15 mm in the solution. Nanodiamond particles are positively charged in the solution due to free protons, which are produced by the following reaction [11]

$$CH_3COCH_3 \leftrightarrow CH_3C(OH)CH_2,$$

$$CH_3C(OH)CH_2 + I_2 \rightarrow CH_3COCH_2I + H^+ + I^-,$$

and are attached to nanodiamond particles. Judging from SEM observations on the cathode and anode after electrophoretic deposition, we note the presence of nano-

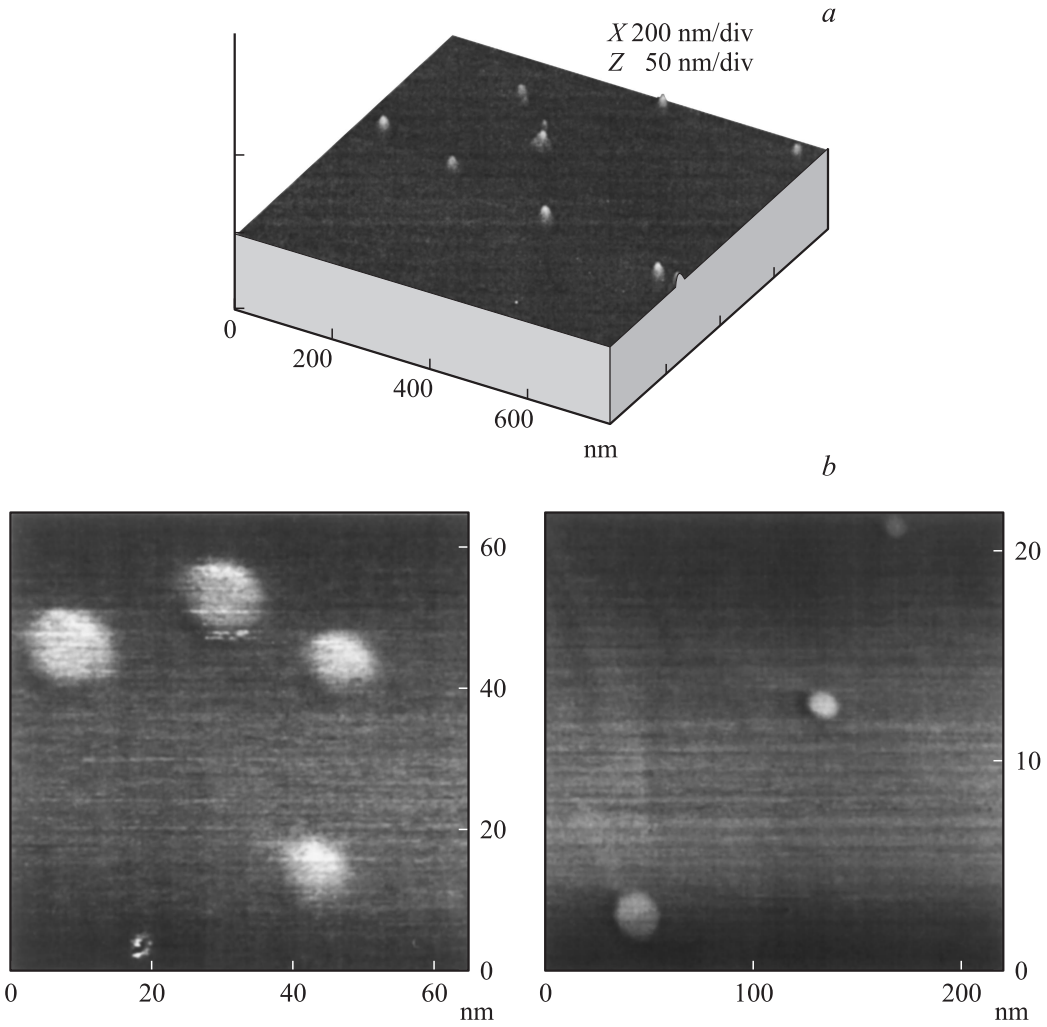

Figure 4. (*a*) AFM image of nanodiamond particles dispersed on a HOPG substrate using electrophoretic deposition. (*b*) STM images of isolated single graphene sheets prepared by the heat treatment of nanodiamond particles at 1600°C.

diamond particles both on cathode and anode. However, the density of particles deposited on the anode is very low ($\sim 10\%$) compared with that deposited on the cathode. These findings suggest that the majority of particles are positively charged with their surface adsorbing H^+ ions, though some particles remain with their original negative surface charge which diamond particles take in pure organic solvents without any additives [12]. Thus, the density of deposited nanodiamond particles is subjected to the concentration of the additives, the voltage applied, and the deposition time. At low applied voltages (~ -0.07 V/cm), the seeding of nanoparticles takes place, whereas high voltages such as -67 V/cm favor an aggregation phenomenon. Interestingly, at very low concentration of iodine (~ 0.1 mg/l), a simple dipping of electrodes in suspension without any applied voltage results in no deposition. This suggests the feasibility of electrophoretic deposition for seeding nanodiamond particles. It is interesting to note that the density of particles decreases as the deposition time increases. This behavior is attributed to a desorption process which occurs simultaneously with the deposition process. In other words, it seems that nanodiamond particles interact weakly with the surface of the substrate, and consequently, spontaneous separations are possible leading to redissolution of particles in the suspension.

The next task is to seed single isolated nanodiamond particles on a substrate from which we obtain isolated single nanographite on the basis of the condition established by the experiments presented above. Isolated nanodiamond particles on a substrate, which are prepared in the condition of 5 mg/l iodine, an applied voltage of -6.67 V/cm and a deposition time of 30 s for this purpose, are imaged by AFM as shown in Fig. 4, *a*. From the observed images, it is revealed that the nanodiamond particles are well dispersed with the interparticle distances far enough to get isolated single particles on the substrate.

The nanodiamond particles are heat-treated in an argon atmosphere for 30 min at HTT = 1600°C, which has been suggested to be an appropriate condition for obtaining nanographite particles from the experiments presented in

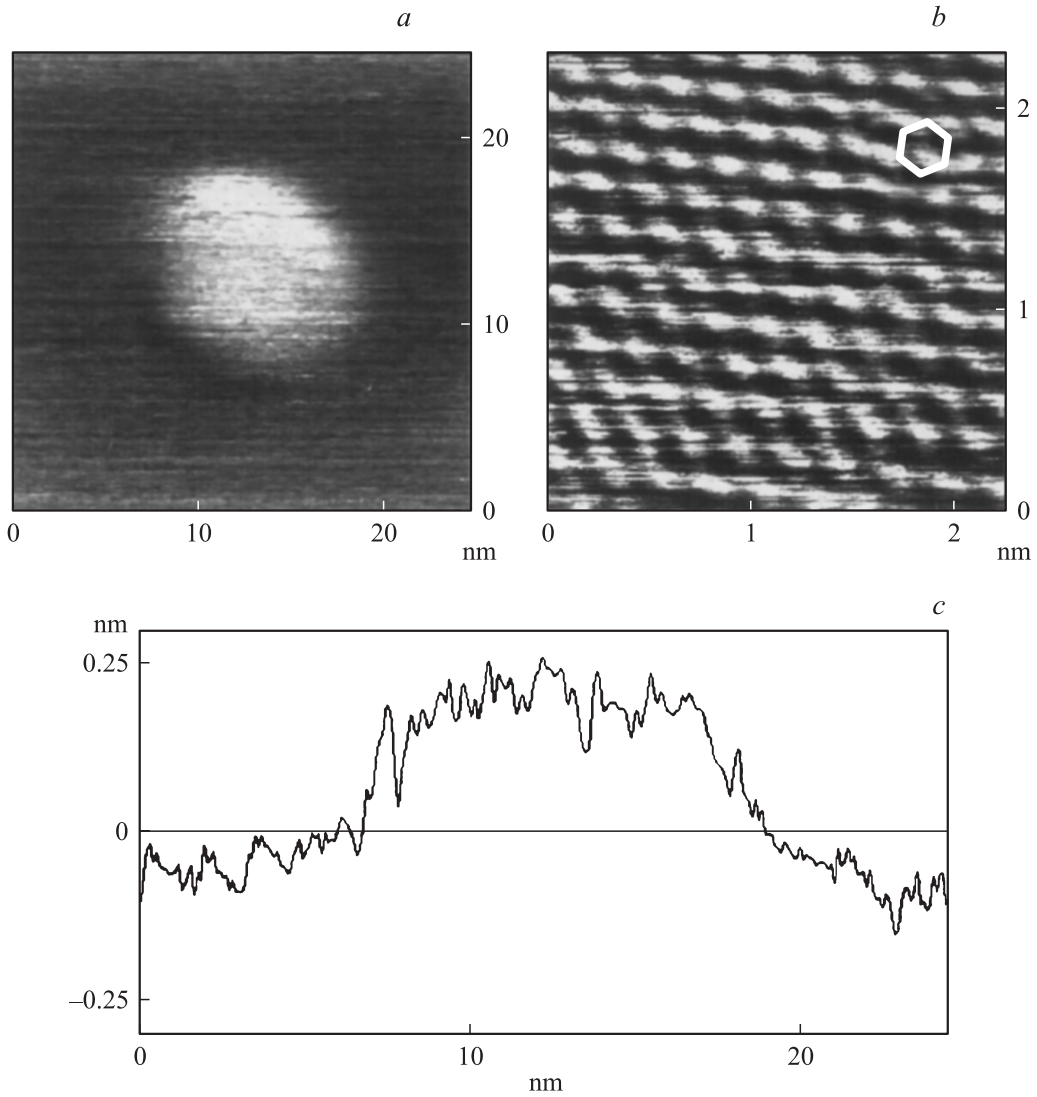

Figure 5. (*a*) Image of a single nanographene sheet, (*b*) the lattice image of a single nanographene sheet, and (*c*) the cross-section analysis. A hexagon represents a benzene ring. The section profile is in horizontal direction across the center of the particle.

the last section. The obtained particles are imaged by STM as shown in Figs. 4, 5 [13]. The particles are flat with their planes being parallel to the HOPG substrate, where a mean in-plane size of the particles is estimated as ca 10 nm. The cross-sectional profile shown in Fig.5, *c* gives the height of the plane from the substrate 0.35–0.37 nm, which is considerably larger than the interlayer distance of bulk graphite (0.3345 nm). Therefore, the obtained particle can be assigned to a single nanographene sheet laying flat on the HOPG substrate. Comparison between the lattice images of the nanographene sheet and the HOPG substrate, which have the in-plane lattice constant of 0.25 nm, suggests that the nanographene sheet is placed eptaxially on the substrate, since the lattice image of the nanographene sheet is well registered to that of HOPG substrate. This is the first observation of a single nanographene sheet to the best of our knowledge. The number of carbon atoms involved in this nanographene sheet is estimated roughly at $N \sim 3000$. From the view point of organic chemistry, this is the largest polycyclic condensed aromatic molecule having ever been observed.

Nanodiamond particles when simply heated at 1600°C yields the polyhedral nanographite particles with a hollow inside as discussed in the last section. It is surprising to obtain a single nanographene sheet instead of spherical or polyhedral nanographite particles. A trace of oxygen in argon gas in the heat-treatment process might have reacted with the surface of diamond and consequently a part of particles is oxidized during the heat-treatment, resulting in the observed flat shape. The surface of a nanodiamond particle in contact with the HOPG substrate is more stable to the oxidation compared to the free exposed part. Also, the part in contact with the HOPG substrate converts to graphite faster than the free part. The newly converted graphite interact with the flat HOPG substrate giving rise to the flat single nanographene sheet.

Finally, we discuss the electronic feature of the nanographene sheet obtained in the experiment. From the observed distance between the nanographene sheet and the substrate, the interlayer interaction (γ_1) becomes reduced by 26–50%, when the interlayer distance is elongated from the bulk to 0.35–0.37 nm, where $\gamma_1 = 0.39$ eV for the bulk. Therefore, the nanographene sheet obtained in the experiment interacts weakly with the substrate, which is absolutely different form graphene layers produced on metal or carbide surface, as the graphene in the latter is subjected to strong electronic interaction with the substrate through the hybridization of the electronic states [14,15].The quantum size effect is also expected to prevail in the electronic structure of the nanographene sheet. The energy discreteness Δ is of the order of W/N where $W\,(=6\gamma_0)$ is the band width of π-band and the intralayer resonance integral is $\gamma_0 = 3.16$ eV. Therefore, the estimated energy discreteness of 75 K is expected to modify the electronic properties at low temperatures through the quantum size effect. More interestingly, from the aspect of electronic features, the present nanographene sheet, which is rather independent from the substrate, will be a good target of investigating the nonbonding edge-state and its related unconventional nanomagnetism.

4. Summary

Heat-treatment-induced conversion of nanodiamond particles having a mean size of ca 5 nm to nanographite in an argon atmosphere is investigated from structural and electronic aspects. Graphitization starts at the surface region around HTT = 900°C, then it proceeds inward in the particle, and finally it is completed around HTT = 1600°C, where nanographite particles form a polyhedron with a mean size of ca 7 nm and a hollow inside. The change in the electronic feature is subjected to the structural change induced by the heat treatment. In the intermediate stage of graphitization, where graphene sheets are small and defective, charge transfer takes place from graphitic π-band to non-bonding edge states. Electrophoretic deposition of nanodiamond particles provides technique of fabricating single isolated nanodiamond particles on a HOPG substrate. Successive heat-treatment at HTT = 1600°C converts a nanodiamond particle to a single nanographene sheet laying flat on a HOPG substrate. A mean size of the nanographene sheets obtained is estimated as ca 10 nm, suggesting the presence of ca 3000 carbon atoms in a sheet. This is the largest condensed polycyclic aromatic molecule in the organic chemistry language having ever reported. A weak interaction between the nanographene sheet and the substrate, which is reduced by 25–30% compared to bulk graphite, is expected to give a model system of nanographene, in which theory predicts the presence of nonbonding π-electron states of edge origin and its related unconventional nanomagnetism.

Acknowledgements

The author would express his sincere thanks to B.L.V. Prasad, A.M. Affoune, H. Sato, A.M. Rao, P.C. Eklund, K. Oshida, M. Endo, Y. Hishiyama, and Y. Kaburagi, on the basis of whose contributions the present work has been carried out.

References

[1] P.K. Baumann, R.J. Nemanich. Surf. Sci. **320**, 409 (1998).
[2] K. Kusakabe, M. Maruyama. Phys. Rev. B **67**, 092 406 (2003).
[3] M. Fujita, K. Wakabayashi, K. Nakada, K. Kusakabe. J. Phys. Soc. Jpn. **65**, 1920 (1996).
[4] K. Wakabayashi, M. Fujita, H. Ajiki, M. Sigrist. Phys. Rev. B **59**, 8271 (1999).
[5] O.E. Andersson, B.L.V. Prasad, H. Sato, T. Enoki, Y. Hishiyama, Y. Kaburagi, M. Yoshikawa, S. Bandow. Phys. Rev. B **58**, 16 387 (1998).
[6] Y. Shibayama, H. Sato, T. Enoki, X.X. Bi, M.S. Dresselhaus, M. Endo. J. Phys. Soc. Jpn. **69**, 734 (2000).
[7] B.L.V. Prasad, H. Sato, T. Enoki, Y. Hishiyama, Y. Kaburagi, A.M. Rao, P.C. Eklund, K. Oshida, M. Endo. Phys. Rev. B **62**, 11 209 (2000).
[8] V.Yu. Osipov, K. Takai, K. Takahara, T. Enoki, M. Endo, T. Hayashi, Y. Hishiyama, Y. Kaburagi, A.Ya. Vul′. Private communication.
[9] G.K. Walters, T.L. Estle. J. Appl. Phys. **32**, 1854 (1961).
[10] A.M. Affoune, B.L.V. Prasad, H. Sato, T. Enoki. Langmuir **17**, 547 (2001).
[11] N. Koura, T. Tsukamoto, H. Shoji, T. Hotta. Jpn. J. Appl. Phys. **34**, 1643 (1995).
[12] J.L. Valdes, J.M. Mitchel, J.A. Mucha, L. Seibles, H. Higgins. J. Electrochem. Soc. **138**, 635 (1991).
[13] A.M. Affoune, B.L.V. Prasad, H. Sato, T. Enoki, Y. Kaburagi, Y. Hishiyama. Chem. Phys. Lett. **348**, 17 (2001).
[14] N.R. Gall, E.V. Rut′kov, A.Y. Tontegote. Int. J. Mod. Phys. **11**, 18 (1997).
[15] C. Oshima, H. Itoh, T. Ichinokawa, T. Aizawa, R. Souda, S. Otani, Y. Ishizawa. Ordering at surfaces and interfaces / Ed. A. Yoshimori, T. Shinjo, H. Watanabe. Springer, Berlin (1992). Vol. 5. P. 13.